Available on CMS information server

**CMS NOTE -2009/022**

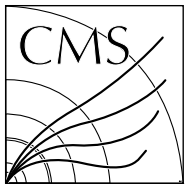

**The Compact Muon Solenoid Experiment**

# CMS Note

Mailing address: CMS CERN, CH-1211 GENEVA 23, Switzerland

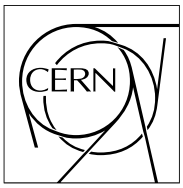

**12 August 2009 (v2, 30 November 2009)**

# Results from a Beam Test of a Prototype PLT Diamond Pixel Telescope

R. Hall-Wilton, R. Loos, V. Ryjov

*CERN, Geneva, Switzerland*

M. Pernicka, S. Schmied, H. Steninger

*Institute of High Energy Physics, Vienna, Austria*

V. Halyo, B. Harrop, A. Hunt, D. Marlow, B. Sands, D.Stickland

*Princeton University, Princeton, NJ, USA*

O. Atramentov, E. Bartz, J. Doroshenko, Y. Gershtein, D. Hits, S. Schnetzer, R. Stone

*Rutgers University, Piscataway, NJ, USA*

P. Butler, S. Lansley, N. Rodrigues

*University of Canterbury, Christchurch, New Zealand*

W. Bugg, M. Hollingsworth, S. Spanier

*University of Tennessee, Knoxville, TN, USA*

W. Johns

*Vanderbilt University, Nashville, TN, USA*

**Abstract**

We describe the results from a beam test of a telescope consisting of three planes of single-crystal, diamond pixel detectors. This telescope is a prototype for a proposed small-angle luminosity monitor, the Pixel Luminosity Telescope (PLT), for CMS. We recorded the pixel addresses and pulse heights of all pixels over threshold as well as the fast-or signals from all three telescope planes. We present results on the telescope performance including occupancies, pulse heights, fast-or efficiencies and particle tracking. These results show that the PLT design concept is sound and indicate that the project is ready to proceed with the next phase of carrying out a complete system test, including full optical readout.

# 1 Introduction

The Pixel Luminosity Telescope (PLT) is a proposed dedicated luminosity monitor for CMS based on single-crystal diamond pixel sensors. The PLT is comprised of two arrays of eight small-angle telescopes situated one on each end of CMS. The telescopes consist of three equally-spaced planes of diamond pixel sensors with a total telescope length of 7.5 cm. They are located 5 cm radially from the beam line at a distance of 1.8 m from the central collision point. Figure 1 shows a sketch of a PLT array and indicates its location within CMS. The telescope planes consist of single-crystal diamond sensors with active area of 3.6 mm $\times$ 3.8 mm that are bump bonded to the PSI46v2 CMS pixel readout chip[1]. The PLT is designed to provide a high-precision measurement of the bunch-by-bunch relative luminosity at the CMS collision point on a time scale of a few seconds and a stable high-precision measurement of the integrated relative luminosity over the entire lifetime of the CMS experiment.

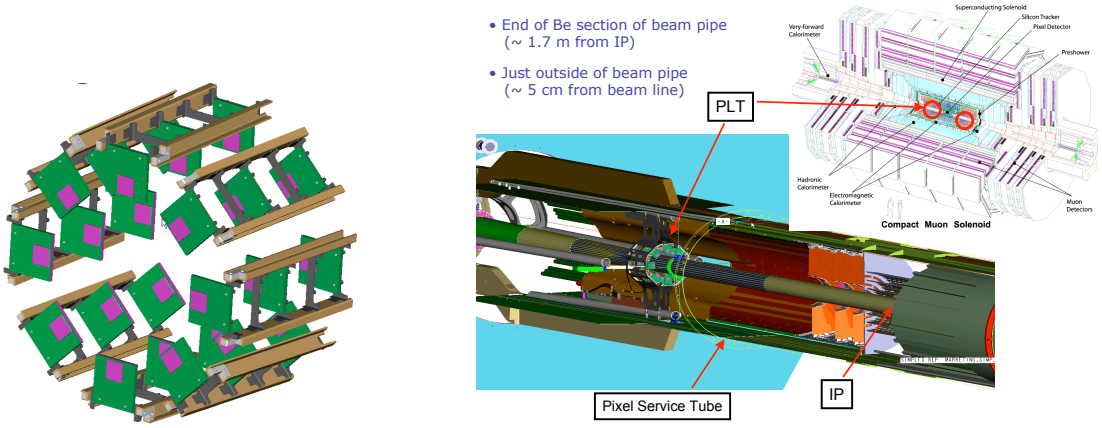


Figure 1: Sketch of one of the PLT telescope arrays and its location within CMS. The magenta squares on the telescope planes indicate the locations of the diamond sensors.

The primary luminosity measurement of the PLT is based on counting the number of telescopes with three-fold coincidences formed from the fast-or, column-multiplicity signal output by the PSI46 readout chip. The fast-or signal, clocked at the bunch crossing rate of 40 MHz, indicates the number of double columns that had pixels over threshold in each bunch crossing. In addition, the full pixel information consisting of the row and column addresses and the pulse heights of all pixels over threshold is readout at a lower rate of a few kHZ. This full pixel readout provides tracking information and is a powerful tool for determining systematic corrections, calibrating pixel efficiencies and measuring the real-time location of the collision point centroid.

Diamond sensors are crucial for the PLT application since they will operate efficiently with only moderate decrease in signal size over the entire lifetime of CMS[2]. Of equal importance, this radiation hardness does not require that the sensors be cooled. Single-crystal diamond is used for the sensor material rather than polycrystalline diamond since the pulse height distribution of single crystal diamond is large and well separated from zero, ensuring that any efficiency changes due to threshold drifts will be small. In order to determine the performance of the diamond pixel sensors and the soundness of the PLT design, we carried out a test of a prototype telescope in a 150 GeV/c $\pi^+$ beam in the H4 beamline of the CERN SPS in May of 2009. The primary goals of this test were to determine: the yield of good pixel channels that result from the bump-bonding process; the pulse height response of the diamond sensors for minimum ionizing particles; the fast-or signal efficiency; and the tracking capability of the diamond pixel planes. Although seven days of beam time had been allocated, we had only two days of beam due to accelerator problems. Despite the limited beam time, we were able to complete the core components of the program, although with considerably less statistics and without the benefit of optimization and tuning of parameters that would have been possible with the full beam time allotment.

# 2 Detector Preparation

The diamond sensors were single-crystal Chemical Vapor Deposition (CVD) diamond with nominal thickness of 500 $\mu$m supplied by Diamond Detectors Ltd. Their physical area of 4.7 mm $\times$ 4.7 mm is the largest size currently available for commercial, single-crystal, detector-grade diamond. Although a larger diamond size would have been preferred for ease of handling during processing, the present area is more than sufficient for the solid angle coverage required for the PLT. The characteristics of each diamond sensor was studied using a $^{90}$Sr beta source.

We found that 15 out of the 32 sensors measured achieved full charge collection at an applied field between 0.05 V/$\mu$m and 0.2 V/$\mu$m with an additional 13 sensors achieving full charge collection at an applied field between 0.2V/$\mu$m and 0.4 V/$\mu$m. For the beam test, a bias voltage of 250 V was applied to each of the three diamond sensor planes corresponding to approximately 0.5 V/$\mu$m.

Deposition of the pixel electrode pattern on the diamonds and the bump-bonding of the diamond sensors to the pixel readout chips were performed "in-house" at the Princeton Institute of Science and Technology Materials (PRISM) micro-fabrication laboratory. Following surface preparation, electrodes were sputtered onto the diamond surface using a Ti/W alloy target as an under bump metalizaztion (UBM). A 4 mm $\times$ 4 mm electrode was deposited on one side of the diamond using a shadow mask. On the other side, a pixel pattern was deposited using a standard lift-off photolithographic process. The pattern covered an area of 3.9 mm $\times$ 4.0 mm and consisted of an array of 26 $\times$ 40 pixels with pitch of 150 $\mu$m $\times$ 100 $\mu$m matching that of the PSI46 chip. Each UBM pixel electrode was 125 $\mu$m $\times$ 75 $\mu$m with 25 $\mu$m gaps between electrodes. The pixelated diamond sensors were then bump-bonded to the readout chip using a flip-chip procedure. Approximately cylindrical indium bumps with diameters of 15 $\mu$m and heights of 7 $\mu$m to 8 $\mu$m were evaporated onto the pixel pads on both the readout chip and the diamond sensor, Figures 2. This step required a thick layer of photoresist built up from two layers of intermediate thickness. Depositing the indium bumps on readout chip wafers using this thick photolithographic process was relatively straightforward since chips at the periphery of the wafer could be sacrificed. Depositing the indium bumps on the individual diamond pieces required considerably more development. It was necessary to remove a thick meniscus of photoresist that forms at the edge of the diamond during the photoresist spinning process without compromising the integrity of the pixel pattern close to the edge of the diamond. A procedure was developed for forming a custom-fit frame around each diamond so that the photoresist would fully spin off the diamond onto the sacrificial frame leaving a uniform layer on the diamond. After indium bump deposition, the diamond sensors were then bump-bondied to the readout chip using a Research Devices MA-8 flip-chip bonder with an optically-controlled alignment precision of better than 2 $\mu$m. The electromechanical bond was formed by applying pressure only. The indium bumps were not reflowed. The readout chip has an array of 52 $\times$ 80 channels larger in area than the diamond sensors. The diamonds were bonded to columns 13 through 38 and rows 41 through 80 at the top edge readout chip as seen in Figure 2.

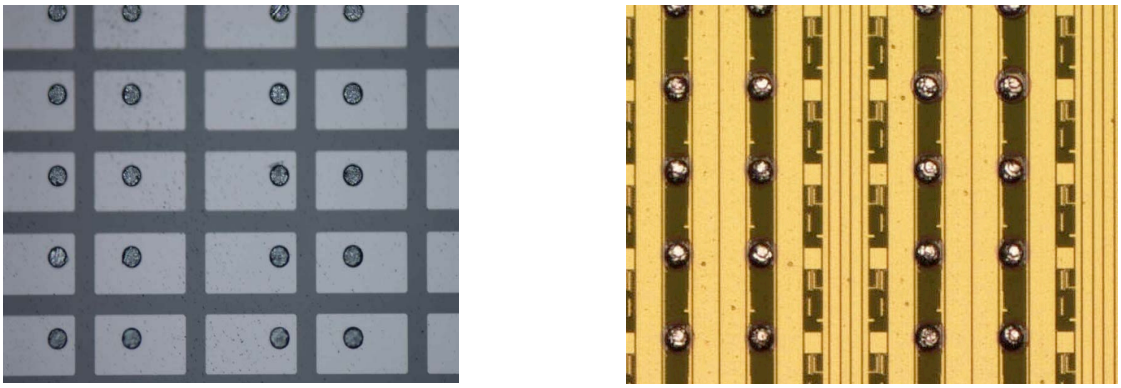

Figure 2: Indium bumps on diamond sensor (left) and readout chip (right).

The bonded detectors were mounted onto hybrid boards consisting of flex circuits with a ceramic filled fiberglass backing to form the telescope planes. The hybrid board had pads for wire bonding of the readout chip, a circuit for distributing the sensor bias voltage and a flex pigtail for connecting to a High Density Interconnect (HDI) circuit that forms the backbone of a telescope. After being qualified using a $^{90}$Sr source, three detector planes were assembled into a telescope. The HDI circuit was placed into a carbon fiber support ladder and each of the three hybrid boards was connected to the HDI. Figure 3 shows a picture of an assembled telescope. The entire telescope assembly consisting of the bump-bonded detector, hybrid board, HDI and carbon fiber ladder is a full PLT prototype. For the test beam, the telescope assembly was inserted into an aluminum cartridge frame pictured in Figure 4. In the PLT, the carbon fiber ladder will instead be inserted directly into a slot in the PLT support carriage.

All columns of all three diamond detector planes were operational except for the five left-most columns of Plane 1. The diamond sensor for this plane had a significant wedge shape varying by about 50 $\mu$m in thickness from one edge of the diamond to the other. This caused difficulty in the flip-chip bonding. In the first attempt nine columns did not form bonds. The sensor and readout chip were separated and in a second bonding attempt all columns

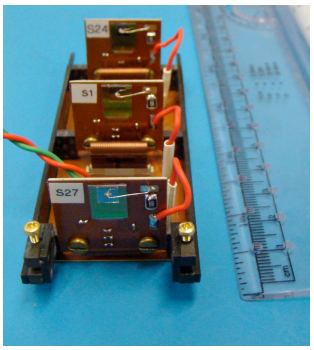


Figure 3: Assembled telescope.

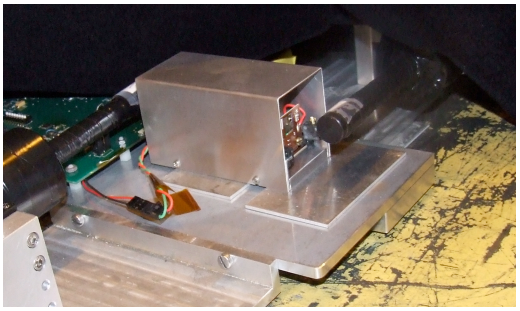

Figure 4: Telescope in test beam with upstream and downstream trigger scintillators.

bonded except for left-most five. This wedging was due to a temporary defect in the polishing procedure that has since been corrected.

# 3 Detector Readout

A block diagram of the readout scheme used in the beam test is shown in Figure 5. The front-end part of the readout chain consisting of the readout chip, hybrid board and HDI circuit represents closely the circuitry that will be used in the PLT. The hybrid board was described above. The three hybrid board planes that make up a telescope are connected by pigtails to the HDI, a four-layer flex circuit. The HDI houses a CMS pixel Token Bit Manager (TBM) chip that communicates with the three readout chips in the telescope and orchestrates readout of the full pixel information. This data is output by the TBM onto a single analog line. The HDI also houses a custom PLT driver chip that amplifies and outputs the three fast-or signals onto separate analog lines. The HDI also distributes low voltage power and sensor bias voltage to the hybrid boards.

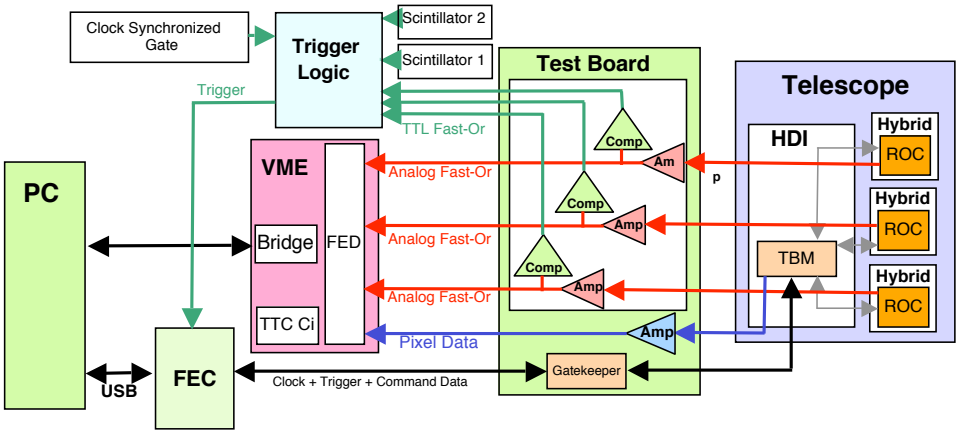


Figure 5: Block diagram of DAQ readout chain.

The port card and opto board are closely coupled to mechanical design constraints of the PLT support structure and along with the rest of the optical part of the readout chain are currently under design. For the beam test, the readout downstream of the HDI was, therefore, electrical rather than optical. The HDI was connected to a telescope test stand board that played the role of the port card. This board produced four amplified, single-ended analog signals from four differential analog signals: one full pixel readout signal from the TBM and three fast-or signals, one from each of the three readout chips. These signals were sent on coaxial cables, approximately 30 m long, to the electronics control room. The test stand board also output a digital TTL signal for each of the three fast-or signals for use in triggering. A Front End Controller (FEC) test stand board provided functions similar to those of the FEC module of the CMS pixel detector. It programed the registers in the TBM and readout chips and set the pixel threshold trim values. It also sent clock and trigger signals to the TBM. The telescope test stand board was located in the beam line next to the telescope while the FEC board was located 30 m away in the electronics control room.

The full readout pixel analog signal and the three fast-or signals were input to the FED flash-ADC module. This FED was a modified version of the CMS pixel system FED that accepted electrical rather than optical inputs. The module was otherwise identical to the FED used for the CMS pixel systems. The whole system including readout chips, TBM chip and FED was clocked at 40 MHz.

Figure 4 shows the setup in the beam line. Small scintillators each 8 mm $\times$ 8 mm, seen in the figure, were positioned just upstream and downstream of the telescope. All of the results reported here are based on events triggered by a coincidence of these two scintillators. When a trigger coincidence occurred a signal was sent to the FED via a CMS Timing Trigger and Control Interface ($TTC_{ci}$) module initiating digitization. In order to have a wide time view of the event, the digitization started three clock periods before the event and continued for 960 clock periods.

Before taking data, a procedure, similar to that for the CMS pixel detectors, was used to lower the pixel thresholds as much as possible. This was a multiple-step procedure that involved adjusting three DAC settings in the readout chip: the overall course threshold, the trimming range around this setting and the trimmed threshold for each individual pixel. The pixel thresholds achieved were in the range of 2,500 to 4,500 electrons as noted below.

The telescopes planes were calibrated using the built-in pulsing capability of the PSI46 readout chip. Internally the readout chip could be programmed to deposit known amounts of charge into selected pixel channels. One-by-one each pixel was calibrated by ramping this charge through the full input range while reading the output signal into the FED. The input charge was plotted vs. the FED ADC value and fit to a second-order polynomial to obtain a mapping from ADC count to pulse height in electrons.

# 4 Results

Here we present results from the beam test on pixel occupancies, tracking, pulse heights and fast-or efficiencies.

## 4.1 Plane Occupancies and Pixel Yield

Figure 6 shows the occupancy of each of the three telescope planes for events triggered by a coincidence of the two 8 mm $\times$ 8 mm scintillators. The area of each pixel box in the figure is proportional to the number of hits on the pixel. As noted above, the first five columns of Plane 1 were disabled because of bonding problems caused by the wedge shape of this sensor. Due to several noisy pixels, the rightmost column of Plane 1 was also disabled. All of the rest of the columns in all three planes were enabled. Because of limited beam time, we were not able to fully iterate the alignment of the telescope and scintillators with beam. As a result, the leftmost columns of the telescope planes were not covered by the scintillators, as can be seen in the figure. Since the telescope was not perfectly aligned with the beam, the scintillator coverage varied by plus or minus one column among the three planes. The outermost rows and columns collect charge from particles over a region extending outside of the pixelized region and, therefore, have more hits than other rows and columns. In the PLT, these outermost rows and columns will be masked in order to define a sharp fiducial region given by the boundary between the outermost rows (columns) and their neighboring row (column). Figure 7 shows the same plots but with the outermost rows and columns and the columns not covered by the scintillators left blank.

In all three planes, pixels in Row 78 also tend to have a larger number of hits than other rows. This is not currently understood but may be related to the fact that the diamond is mounted close to the edge of the readout chip. The six empty pixels in Column 37 of Plane 1 were noisy and were masked off.

Except for shadowed and disabled columns, nearly all pixels were active. Figure 8 shows the distribution of the number of hits per pixel for those pixels in the non-blanked columns in Figure 7. The number of pixels without any hits are 1.8%, 2.2% and 0.1% for Planes 1, 2 and 3, respectively, indicating that, for these planes, the yield of good pixel bump connections was 98% or better. Since the time that these sensors were bump-bonded, we have continued to improve and gain experience with the process and expect that the current percentage yield of good bump connections is even higher.

## 4.2 Tracking

In order to reconstruct tracks in the telescope, we first found the clusters associated with particle hits in each plane. Pixels above threshold that were nearest neighbors in either the row or column direction were merged. Figure 9

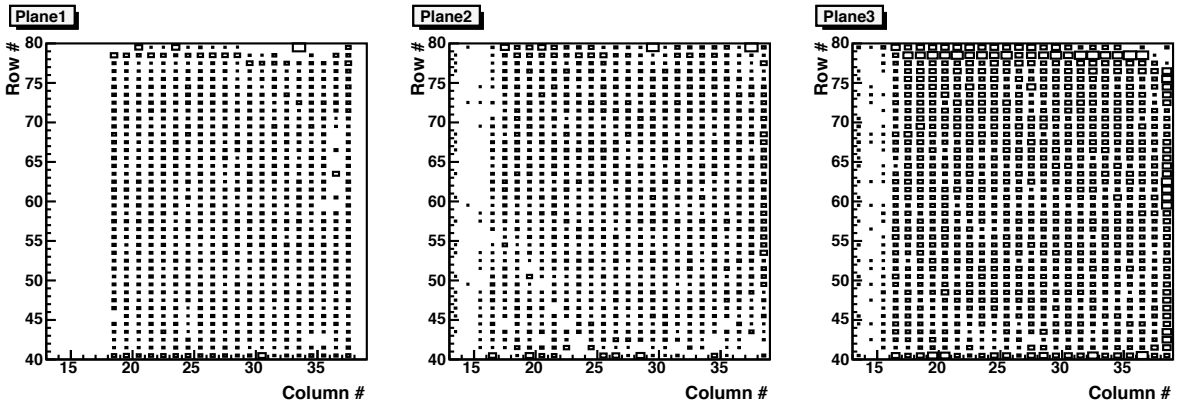


Figure 6: Occupancy map for each of the three telescope planes. Area of each pixel box is proportional to the number of hits on the pixel.

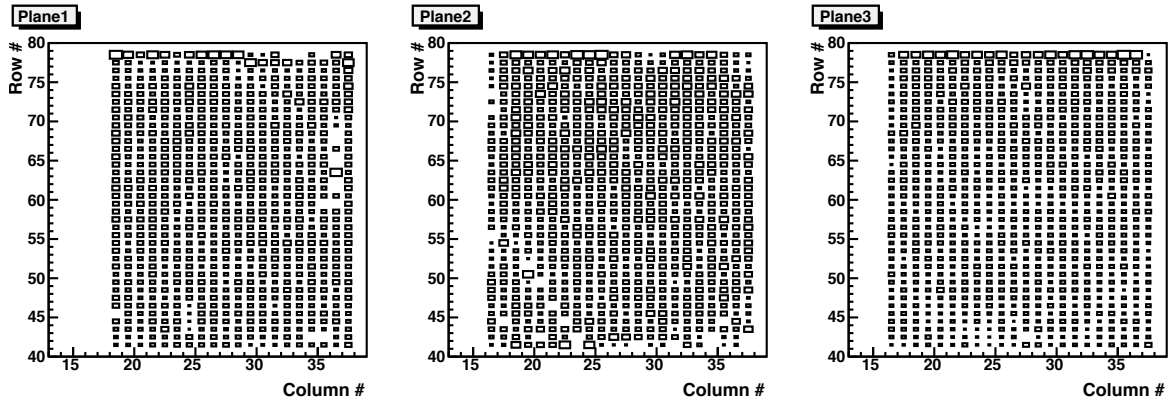


Figure 7: Occupancy map for each of the three telescope planes with border and shadowed pixels left unfilled.

show the distributions of the number of pixels per cluster for each of the three planes. For our analysis, clusters in which three or more pixels were aligned in either a row or column were excluded. The resulting clusters consisted of one, two, three or four nearest neighbor pixels. The cluster position was calculated as the average of the positions of its constituent pixels weighted by their collected charge. Figure 10 shows a sample of tracks reconstructed from the cluster positions. For this plot, events were selected in which there was one and only one cluster in each of the three planes. Events of this type constitute 89% of events that have an in-time fast-or signal in all three planes. The different colors indicate different events. The lines shown are linear fits to the cluster hit positions. Figure 11 shows a similar sample of tracks in a three-dimensional display.

The tracking information allowed us to readily determine the relative alignment of the three planes. Using the difference between the hit cluster position in Plane 2 and the average of the hit cluster positions in Planes 1 and 3, we determined the relative offset of Plane 2 with respect to Planes 1 and 3. This offset was 25 $\mu$m $\pm$ 5 $\mu$m

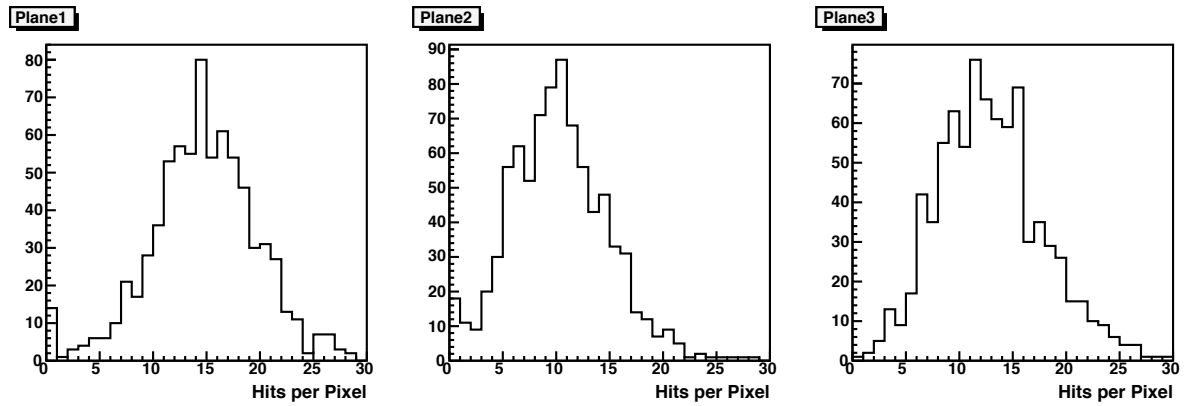


Figure 8: Distribution of the number of hits per pixel for each of the three telescope planes.

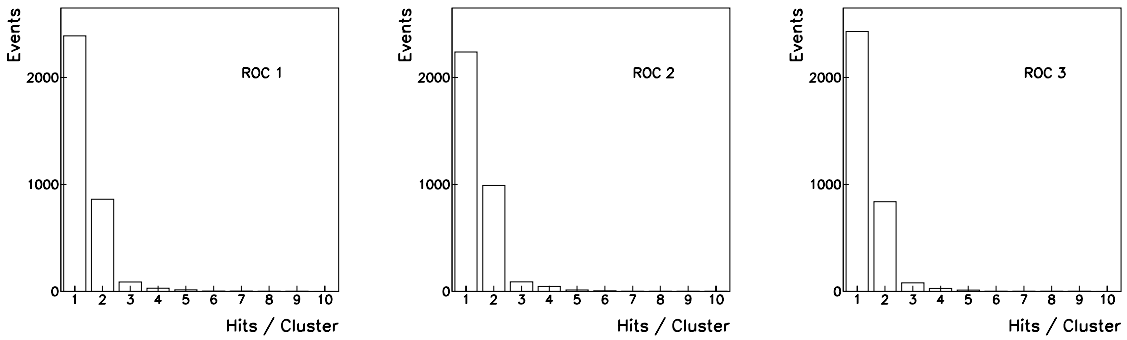


Figure 9: Number of pixels (hits) per cluster for each of the three planes.

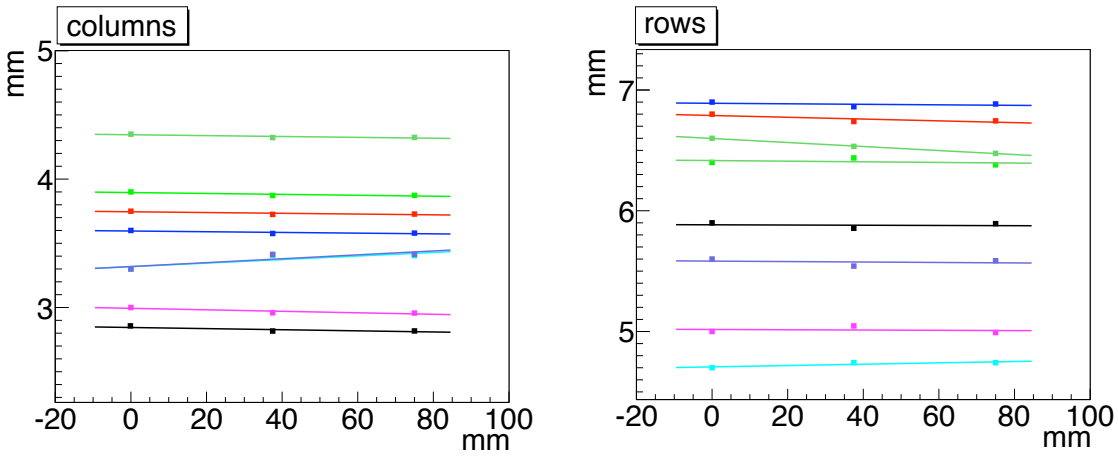


Figure 10: A sampling of tracks reconstructed in the telescope. Each color represents a different event. The lines are linear fits to the cluster hit positions.

in the column direction and 146 $\mu$m $\pm$ 3 $\mu$m in the row direction. Although it is only one data point, it gives an indication of the accuracy of the positioning of detectors onto the telescope planes and of the planes into the telescope during the assembly process. The accuracy indicated here is well within that required for the PLT. In addition, the difference of the hit cluster positions in two planes vs. the hit cluster position in the orthogonal direction allowed us to determine the relative rotation of the three planes about the beam direction. The largest was a rotation of Plane 2 by 0.6 degrees with respect to Planes 1 and 3. This alignment of the telescope planes was done readily with only a small amount of data indicating that the alignment of the PLT will be straightforward and quick once data comes.

Hit residuals indicate that the spatial resolution is better than digital, pixel width divided by $\sqrt{12}$, as would be expected from the charge sharing reflected in the fraction of two-pixel clusters seen in Figure 9. With the current data, though, we are not able to measure the spatial resolution of the detector planes. That would require either that the planes be rotated with respect to the beam or that an external strip-tracking telescope be used for independently determining track hit positions. In this test beam run, we had the capability of rotating the planes by 20 degrees with respect to the beam but didn't have sufficient beam time to take data with this run condition. While spatial resolution is not a key aspect for the functioning of the PLT, we are considering a future beam test with rotated planes and external tracking telescope for measuring it.

## 4.3 Pulse Height Distributions

For determining pulse height distributions, we defined an acceptance region in each of the three planes such that if a beam particle were incident on this region in two of the planes it was certain to also be incident on the enabled area of the third plane. Figure 12 shows these acceptance regions. Because the telescope was at a slight angle with respect to the beam, there was an approximately 8 row offset between Planes 1 and 3 in particle hit position. Figure 13 shows the summed pulse height distributions in units of collected electrons for each of the three planes where for a given plane a cluster within the acceptance region of the other two planes was required. We also required that

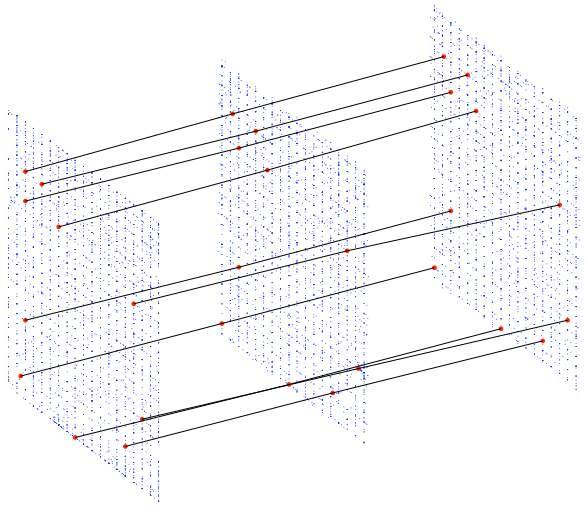

Figure 11: A three-dimensional display of tracks. The lines drawn connect the cluster hit positions.

there be one and only one cluster in each of these two planes. The pulse height plotted is the sum over all pixels within the hit cluster. The most probable signal is approximately 16,000 electrons for Plane 1 and approximately 18,500 electrons for Planes 2 and 3. There is a 10% systematic uncertainty in calibration from plane to plane. For comparison, the most probable signal for a 300 $\mu$m thick silicon sensor is 22,000 electrons. The most probable pulse height in Plane 1 is about 15% lower than that for Planes 2 and 3. This is largely due to the fact that the average thickness of the diamond sensor for this plane was less than that of the other two. Planes 2 and 3 were 499 $\mu$m and 496 $\mu$m, respectively while Plane 1 was wedge-shaped and had an average thickness of 457 $\mu$m with a variation of 50 $\mu$m from one side to the other. The small bump in the pulse height distribution of Plane 2 at around 5,000 electrons is not yet fully understood but seems to be due to about fifteen pixels that have anomalously low pulse heights.

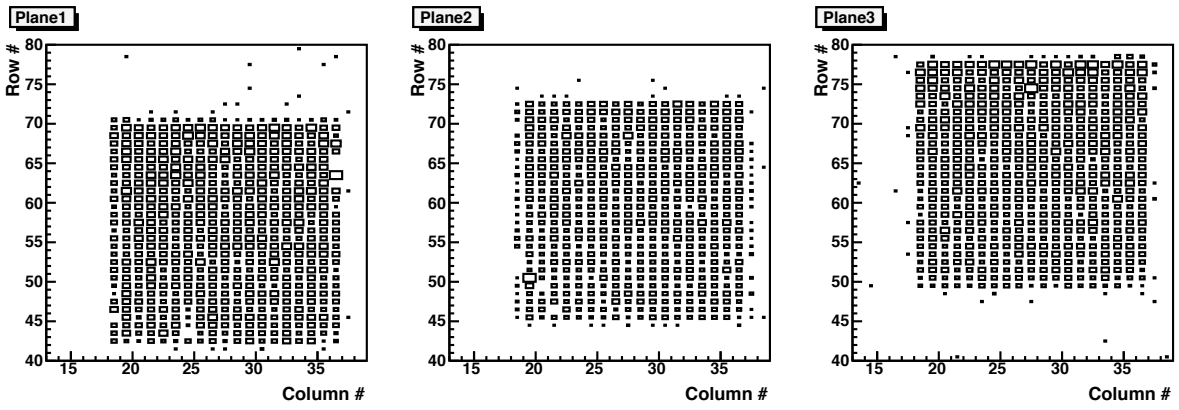


Figure 12: Acceptance regions of the three planes.

We can obtain a measure of the pixel threshold settings by examining the turn on of the distribution for low pulse heights. Figure 14 shows the pulse height distributions of the lowest pulse height pixel for the case of two-pixel clusters. Most of these two-pixlel clusters result from charge sharing when the particle hits close to a pixel boundary. These distributions indicate that the threshold turn on is 3,500 to 4,500 electrons, 3,000 to 4,000 electrons and 2,500 to 3,500 electrons for Planes 1, 2 and 3, respectively. Although these threshold are low, if there had been more time to tune and iterate the threshold trimming lower values could likely have been achieved.

## 4.4 Fast-Or Efficiencies

The fast-or signals form the basis for the primary luminosity measurement of the PLT. Clocked at the LHC bunch crossing rate of 40 MHz, they will allow the three-fold coincidence rate within each telescope to be formed for each LHC bunch crossing, thereby, determining the relative bunch-by-bunch luminosity. Understanding these fast-or signals and measuring their efficiency is key to establishing the performance of the PLT. While the fast-or output

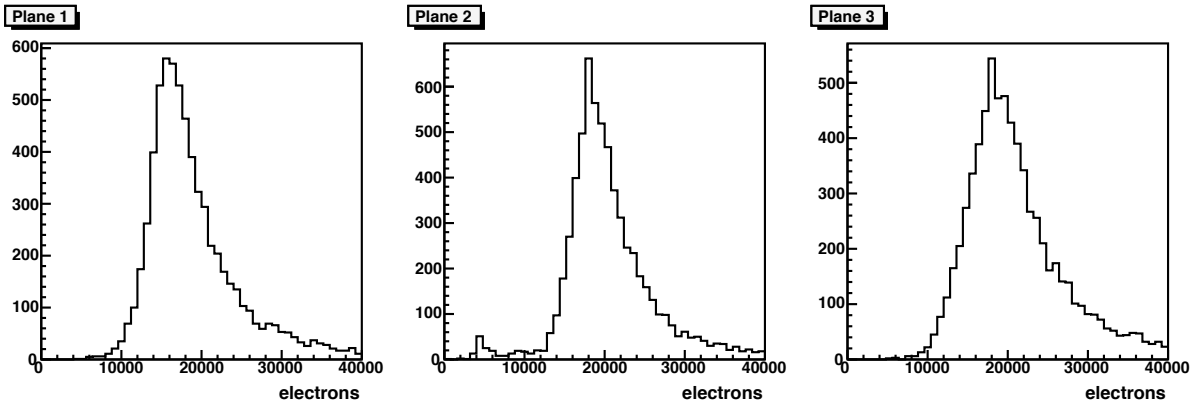


Figure 13: Distribution of the summed pulse height for each of the three telescope planes.

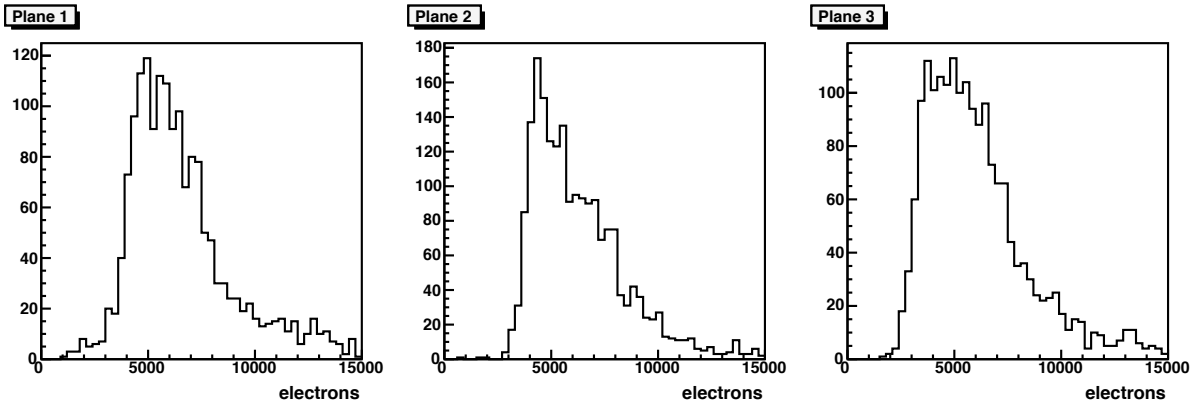


Figure 14: Pulse height distributions for the pixel with lowest pulse height for events in which two pixels are over threshold.

of the PSI46 chip was implemented for possible application in the Level 1 trigger, the current results are the first systematic study of their efficiency.

For determining the fast-of efficiencies, we imposed the same requirements as for the pulse height measurement above in order to ensure that a particle passed through the enabled area of the plane under test. For the two planes other than the one under test, we required that there be only one cluster and that the cluster position be in the acceptance region, see Figure 12 above.

In the test beam, the arrival time of beam particles was asynchronous with the clock phase. Due to time walk, a particle that arrived shortly after the leading clock edge and that had a large pulse height might be output one clock period earlier than the clock time of the trigger. Similarly, a particle that arrived shortly before the trailing clock edge and that had a small pulse height might be output one clock period later than the clock time of the trigger. For the PLT operation at the LHC, the clock will be synchronized with the bunch crossing and particle arrival times will be fixed to within a few nanoseconds relative to the clock edge. The clock phase at the readout chips can then be adjusted so that all of the fast-or signals will occur in the "in-time" clock pulse. For the test beam data, in order to correctly determine the fast-or efficiency, it is necessary to count fast-or signals that occur one clock period early or one clock period late as well as those that occur in-time. The fast-or efficiencies and the percentage of events with early-only or late-only fast-or signals are shown in Table 1 below. Plane 2 had a significantly larger percentage of early fast-or signals than did Planes 1 and 3. This is most likely simply an adjustment issue. Given the abbreviated beam time, we were not able to fully tune the adjustment of the fast-or timing in the pixel readout chips and, as a result, for beam particles arriving near the clock edge, the fast-or from Plane 2 was apt to fire on the earlier clock pulse than were those for Planes 1 and 3. In any future beam test the fast-or timing will be fully adjusted and monitored. In any case, as noted above, early fast-or signals will not be an issue during actual operation of the PLT in CMS.

The correction due to accidental firing of the fast-or signal is negligible. In the nine clock pulses occurring between 2.50 $\mu$s and 2.75 $\mu$s after a triggered event, there were 87 fast-or's out of 100,000 events giving a 0.03% probability

| | Plane 1 | Plane 2 | Plane 3 |
|---|---|---|---|
| Early fast-or only | 0.5% | 21% | 2.5% |
| Late fast-or only | 0.0% | 0.4% | 0.1% |
| Total events | 7,146 | 9,049 | 7,814 |
| Events with no fast-or | 53 | 37 | 7 |
| Efficiency | 99.3% | 99.6% | 99.9% |

Table 1: Fast-or percentages and efficiencies.

for an accidental fast-or in a three clock period.

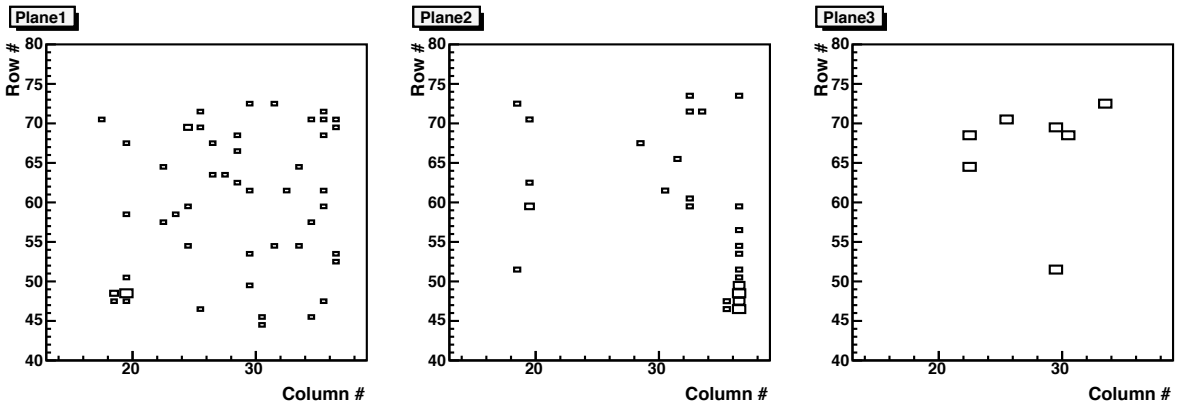


Figure 15: Map of pixels for events with missing fast-or.

Figure 15 shows the hit location in Plane 3 for those events without a fast-or in Plane 1 or Plane 2 and the hit location in Plane 1 for those events without a fast-or in Plane 3. For Planes 1 and 3 there is little correlation with position while for Plane 2 a large fraction of events are in the lower right corner.

Whether in a given event there is a fast-or signal depends on whether the pixel with maximum pulse height is above threshold. Figure 16 shows this maximum pulse height distribution for each of the three planes. These distributions peak well above the measured thresholds indicated in Figure 14 of around 3500 electrons.

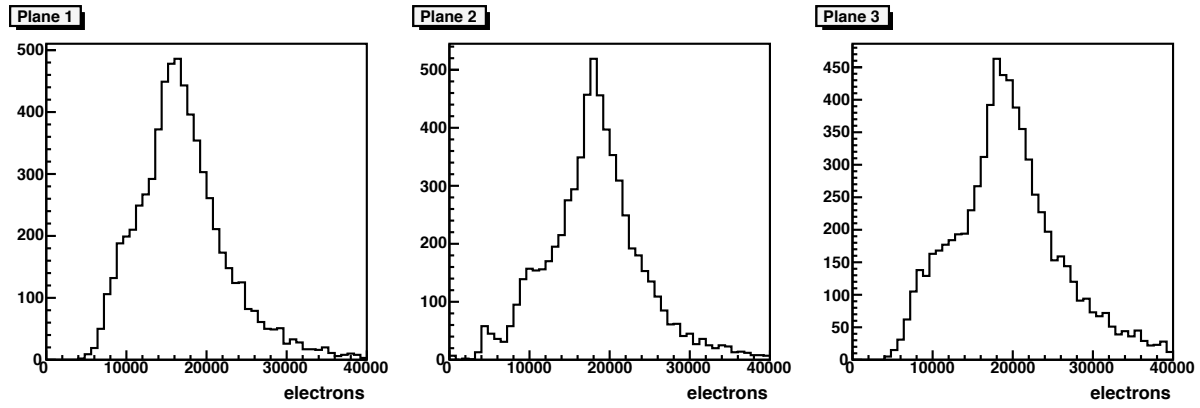


Figure 16: Distribution of pulse height of the pixel with maximum pulse height for each of the three telescope planes.

# 5 Conclusions

We have completed a preliminary analysis of beam test data of a prototype PLT telescope. The fraction of active pixel channels is high, 98% or more, in all three planes. The pulse height distribution for the high energy beam

pions is large with a most probable value of about 18,000 electrons and well above the pixel threshold range of 2,500 to 4,500 electrons. The efficiency of the fast-or signals that form the basis of the primary PLT luminosity measurement is high, greater than 99% for all three planes. Clear and well defined tracks are readily reconstructed in the telescope. These results show that the PLT design concept is sound and that the project is ready to proceed with the next phase of carrying out a complete system test, including full optical readout, of a set of PLT telescopes.

## Acknowledgements

We would like to thank our colleagues in the CMS Beam and Radiation Monitoring group for their advice and assistance. We are grateful to CMS Technical Coordination for assistance in launching and sustaining the project, particularly in its early phases. We thank the management of the US CMS project for their support of this development phase. We also acknowledge the contribution of the CERN technical teams, in particular the ingenuity and dedication of the accelerator and operations groups. R. Hall-Wilton is grateful for the support of the Israeli Technical Associates Program. Finally, we are very grateful for the important and critical contributions to this project made by Alick Macpherson, Richard Lander, Lalith Perera and Gary Grim.

# References

[1] M. Barbero *et al.*, "Design and test of the CMS pixel readout chip," Nucl. Instrum. Meth. A **517**, 349 (2004).

[2] W. Adam *et al.*, "Radiation hard diamond sensors for future tracking applications," Nucl. Instrum. Meth. A **565**, 278 (2006).

[3] D. Kotlinski *et al.*, "The control and readout systems of the CMS pixel barrel detector," Nucl. Instrum. Meth. A **565**, 73 (2006).